THE ASTROPHYSICAL JOURNAL, 434:536–545, 1994 October 20

THE NEAR-INFRARED STRUCTURE OF M33

MICHAEL W. REGAN[1,2] AND STUART N. VOGEL[1,3]
Department of Astronomy, University of Maryland, College Park, MD 20742
Received 1993 October 27; accepted 1994 April 27

ABSTRACT

We present near-infrared mosaics of J, H, and K emission from the central $15' \times 30'$ in M33 which map the stellar distribution of its disk and spheroidal components. Detailed examination of individual OB associations and population synthesis models show that recent massive star formation contributes significantly to near infrared emission, which must be considered in deriving the stellar mass distribution. The scale length of the exponential disk is less than 6′, shorter than optical scale lengths in part because of a radial gradient in extinction. We identify two grand-design spiral arms with an underlying stellar component in the inner 9′; these terminate near the radius at which the rotation curve begins to flatten. A weak, bar-shaped excess in the stellar mass distribution is present in the inner 1′.5; it is unclear whether this traces the inward extension of the spiral arms or a true bar. We find the spheroidal light is reasonably fitted by a single $r^{1/4}$ distribution with a scale length much longer than previously reported for the central spheroidal component. Including a compact bulgelike component does not significantly improve the fit to the surface photometry indicating that the contribution of a compact bulge component to the spheroidal light must be very low. In previous studies of M33, the ratio of the number of globular clusters to spheroid luminosity was anomalously high. Our more extended spheroid results in a ratio closer to that obtained for other spiral galaxies, although it is still high.

Subject headings: galaxies: individual (M33) — galaxies: stellar content — galaxies: structure — infrared: galaxies

1. INTRODUCTION

Since Hubble (1926) first determined that M33 was external to the Milky Way, its nearby location (840 kpc) (Freedman, Wilson, & Madore 1991) and relatively face-on inclination (56°) have made it an ideal galaxy for the study of galactic structure, yet its basic stellar morphology remains unclear. Most of the investigations into the stellar structure of M33 have used the B band or other optical bands. The optical bands include significant emission from O and B stars if these are present. Since the OB stars are very young and can have a vastly different distribution compared to the older population dominating the stellar mass distribution, tracers less sensitive to the young stars are desirable. In addition, visual extinction can be quite severe, particularly in the dust lanes near spiral arms (Rix & Rieke 1993). The near-infrared is potentially a much better tracer of the stellar mass distribution because the extinction in magnitudes at K band is $\sim 10\%$ of that in B band. Also, the O and B stars are expected to contaminate infrared emission less than optical emission, although their contribution to infrared emission remains poorly determined. With the emergence of large-format infrared arrays, it is now possible to map large regions of a nearby galaxy with seeing-limited resolution in the near-infrared.

Sandage & Humphreys (1980) mapped the spiral arms of M33 using B-band photographic plates and concluded that there are 10 spiral arms, characteristic of flocculent galaxies. On the other hand, Kormendy & Norman (1979) listed M33 as a galaxy with two-armed grand-design spiral structure in the inner region. Kormendy & Norman found that grand-design spiral structure is associated with one of the following: interaction with a close companion, a central stellar bar, or solid body rotation in the region of grand-design spiral structure. They attributed the grand-design structure in M33 to solid body rotation. This explanation is brought into question by a more recent study of M33 which found that the rotation curve in the inner 2 kpc may not be well described by solid body rotation (Wilson & Scoville 1989). Computer-enhanced B-band images of M33 suggest the presence of a bar (Elmegreen, Elmegreen, & Montenegro 1992) which could explain the presence of grand-design spiral structure. However, in a recent H-band investigation of the central region of M33 no bar was detected (Minniti, Olszewski, & Rieke 1993, hereafter MOR). A key distinction between flocculent and grand-design spirals is that the flocculent arms are purely gaseous and are prominent because of recent star formation, whereas the grand-design arms have an underlying enhancement in the stellar density. As discussed above, the near-infrared is the preferred tracer of the stellar mass distribution because it is less affected by extinction and star formation. Similarly, a stellar bar should be most prominent in the near-infrared.

According to van den Bergh (1991) the existence of a bulge in M33 is still controversial. Kent (1987) suggested that the excess light seen near the nucleus is due to spiral structure. Bothun (1992) stated that the excess in the surface brightness in the central regions of M33 could not be fitted by a single $r^{1/4}$ law and may not be a bulge but a large-scale diffuse halo. Bothun (1992) also placed an upper limit on the bulge luminosity of $M_V = -15$ based on 12 μm photometry. MOR used H-band photometry of individual stars near the center of M33 and claim that there is a bulge and that it has undergone recent (<1 Gyr) star formation. M33 provides a unique opportunity to investigate a spiral galaxy with a very small spheroid. The light from the spheroids of late-type galaxies at Virgo distances and beyond is brighter than the disk for only a few pixels on most telescopes, making it difficult to distinguish the effect of

[1] Visiting Astronomer, Kitt Peak National Observatory, National Optical Astronomy Observatories, operated by the Association of Universities for Research in Astronomy, Inc., under contract with the National Science Foundation.

[2] E-mail: mregan@astro.umd.edu

[3] E-mail: vogel@astro.umd.edu

any semistellar nucleus from the spheroidal light. With M33 we can investigate the region outside of the semistellar nucleus where the spheroidal light is still brighter than the disk (<30″). Individual halo stars can be resolved at large galactocentric distances (Mould & Kristian 1986), further constraining the mass distribution. As with the spiral arm and bar structure, near-infrared *JHK* photometry should provide the most reliable tracer of the structure of the central region of M33.

In this paper, we will discuss observations of M33 made in *J*, *H*, and *K* bands with the goal of determining the underlying mass distribution and in particular the location and strength of the spiral arms and basic morphology of the central region. In addition, we will investigate the effect that recent star formation has on near-infrared emission.

2. OBSERVATIONS AND DATA REDUCTION

We observed M33 at the Cassegrain focus of the Kitt Peak 1.3 m telescope with the Simultaneous Quad-Imaging Infared Device (SQIID) (Fowler, Gatley, & Merrill 1990) concurrently in *J*, *H*, *K*, and *L*′-bands. SQIID simultaneously images the same 5.′5 field of view in each band using four 256 × 256 PtSi detectors with 1.″4 pixels. We report here on the *J*, *H*, and *K*-band observations.

We observed on the nights of 1992 September 29 and 30 and October 1. The first and third nights were photometric. For a couple of hours on the second night there was a small amount of cirrus. The seeing was always less than 2″ and was undersampled by the large pixels. We used 5 minute exposures with sky frames taken 30′ beyond the eastern and western ends of each 15′ wide row. Sky frames were taken at the beginning and end of each row of the mosaic, so 50 minutes could elapse between sky frames. Due to the excellent gain stability of the PtSi detectors in SQIID the relatively long time between sky frames is not as severe a problem as it is with other near-infrared detectors. We obtained a mosaic of 114 exposures for the inner 15′ × 30′ of M33, with total integration times for each position ranging from 20 minutes in the north and south to 110 minutes toward the nucleus.

After correcting for the nonlinearity of the detectors (Merrill 1992), the SQIID package within IRAF was used for the remainder of the data reduction. Since data frames record sky counts, object counts, and dark current as shown in equation (1), and the sky is much brighter than the target object, the sky must be carefully removed from the raw data frames. The observed counts in the data frame can be represented as a function of pixel location (x, y) as

$$F[x, y] = G_1[x, y]S_1 + G_1[x, y]O[x, y] + D[x, y] , \quad (1)$$

where G_1 is the gain for the data frame, S_1 is the sky contribution, O is the target object and D is the dark current.

Given the large angular size of M33, there is no place on the object frame where the galaxy does not contribute. Thus, we could not use the method of dithering exposures of the target and forming a sky frame by median filtering the data frames. Therefore, we formed a separate sky frame for each data frame by median filtering the four to six nearest sky exposures. These sky frames contain only sky counts and dark current yielding

$$K[x, y] = G_2[x, y]S_2 + D[x, y] , \quad (2)$$

where K is the sky frame, G_2 is the gain for the sky frame, and S_2 is the sky contribution.

By subtracting the sky frame from the data frame rather than first correcting for the gain and then subtracting a scalar value for the sky, small errors in the measurement of the gain are not important and the dark current contribution cancels:

$$F[x, y] - K[x, y] = G_1[x, y]S_1 - G_2[x, y]S_2 + G_1[x, y]O[x, y] . \quad (3)$$

The gain, G, is determined by using all the sky frames for a night, dividing each by its mean intensity and then median filtering. Dividing equation (3) by G yields the processed frame

$$P[x, y] = \frac{F[x, y] - K[x, y]}{G[x, y]} = \frac{G_1[x, y]}{G[x, y]} S_1 - \frac{G_2[x, y]}{G[x, y]} S_2 + \frac{G_1[x, y]}{G[x, y]} O[x, y] . \quad (4)$$

Thus, if the gain does not change ($G_1 = G_2 = G$), the processed frame will only contain the target object and an offset that is independent of position, $(S_1–S_2)$, which is the difference in the intensity of the sky between the object frame and the sky frame. The change in sky intensity is unknown, which means that the correct zero point for each object frame is initially unknown. In addition, if the gain does change between the object frame and the sky frame, possibly due to a change in the spectral composition of the sky over time, the offset in sky counts between the object frame and the sky frame will vary with position. Significant variations in the gain occurred for several of the *K*-band images, and these were therefore not included in the final mosaics. These variations in gain were probably due to the long time that could elapse between sky and data frames.

Mosaics were created by registering the frames using stars in the region of overlap. The relative offset between frames was then found by comparing frames in their overlap regions. The usual method to create a mosaic is to use one frame as a reference and chain background offsets relative to that frame. This has the disadvantage of propagating errors as the length of the chain increases. Instead, we determined the relative offset between every pair of overlapping frames. These pairs of relative offsets were then used as input to a χ^2 minimization routine that solved for the zero point offset for each frame. This method also provides an objective method for rejecting bad frames since these show large residuals. We rejected frames with residual errors more than 3 σ above the mean residual error. This method led to much better results than the single reference frame method since all the available information is utilized and errors do not propagate. Since each of the object frames has an unknown offset and only the relative offsets can be determined using overlap regions, there is still one unknown, the offset to the correct zero point. Given that the average value of $(S_1–S_2)$ for all the frames should be zero, we set the zero point so that the mean of the relative offsets in each band was zero (Quillen, Graham, & Frogel 1993). A mosaic for each filter was formed by merging the individual frames using a median filter in the overlap regions and masking out the bad pixels during the combination process.

We then transformed the *J* mosaic to right ascension and declination using the known positions of stars in M33 (Wilson 1990; Regan & Wilson 1993) and registered the *H* and *K* mosaics with the *J* mosaic.

3. RESULTS

Figures 1*a*–1*c* (Plates 24–26) shows the mosaics for *J*, *H*, and *K*-bands. The stellar disk of M33 is detected over the entire

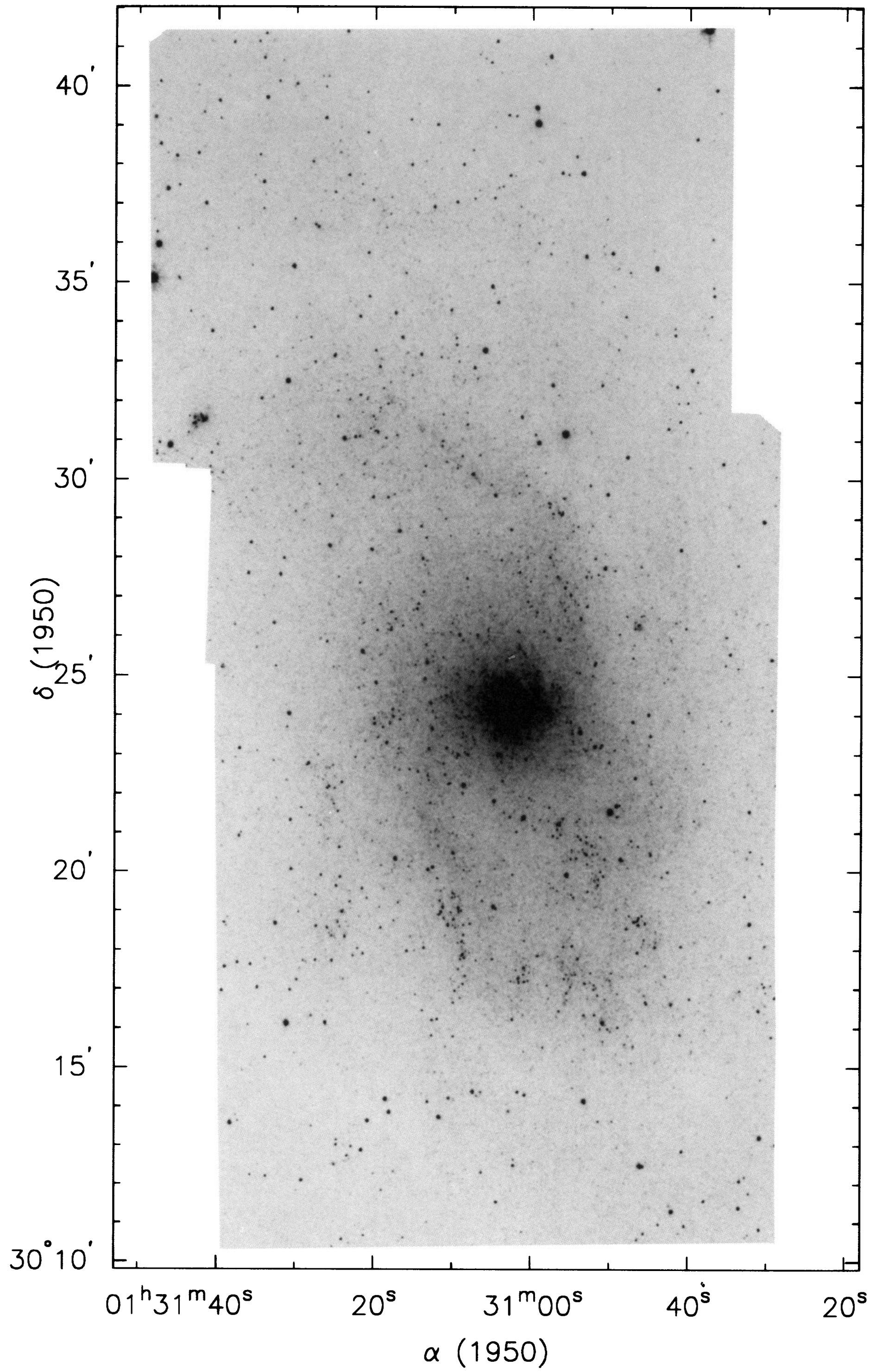

FIG. 1*a*

FIG. 1.—Near-infrared mosaics of the inner 15′ × 30′ of M33. The total integration times range from 100 minutes in the nucleus to 20 minutes in the northern-most row. (*a*) *J*-band (λ midpoint = 1.27 μm), (*b*) *H*-band (λ midpoint = 1.67 μm), (*c*) *K*-band (λ midpoint = 2.22 μm).

REGAN & VOGEL (see 434, 537)

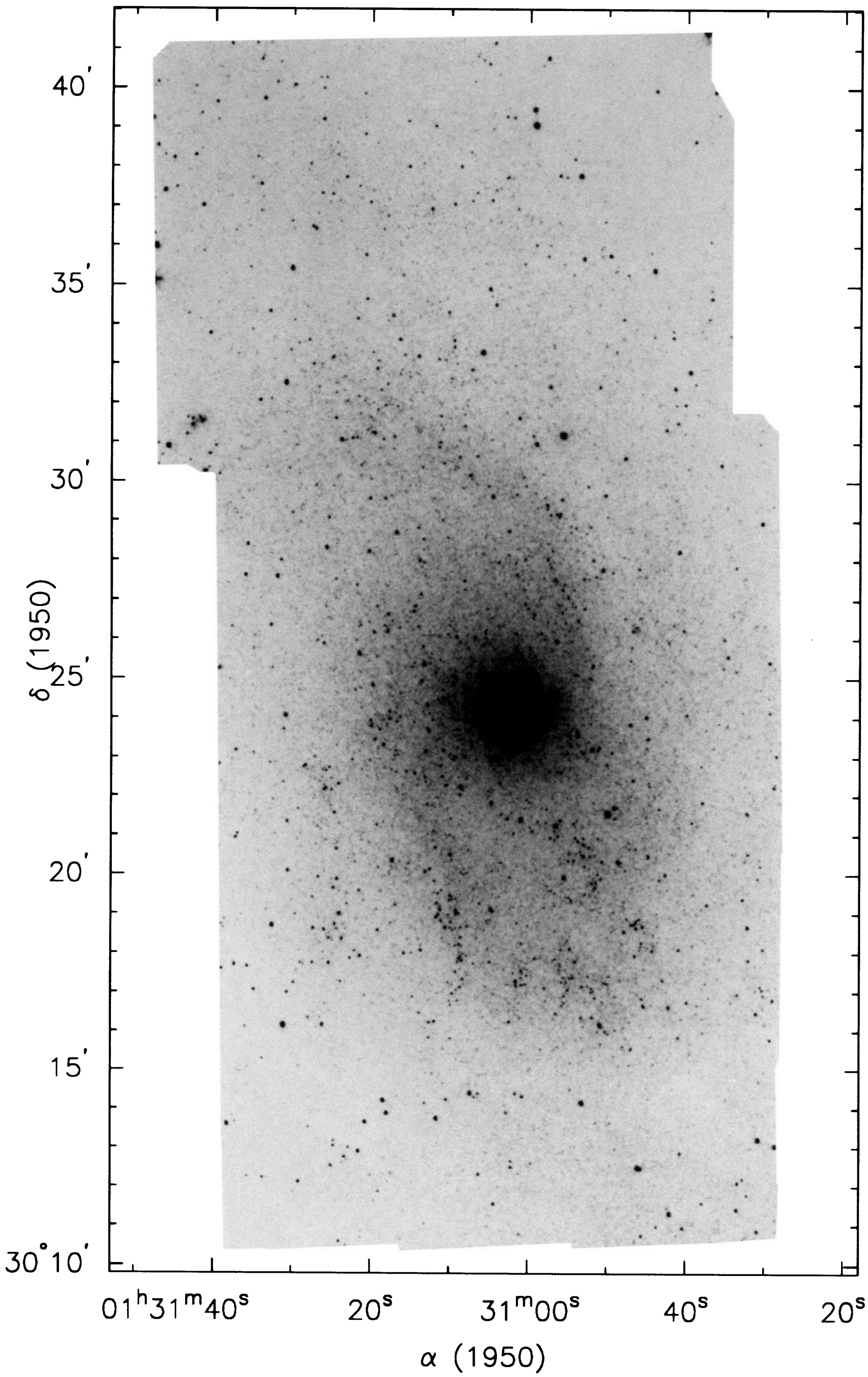

FIG. 1*b*

REGAN & VOGEL (see 434, 537)

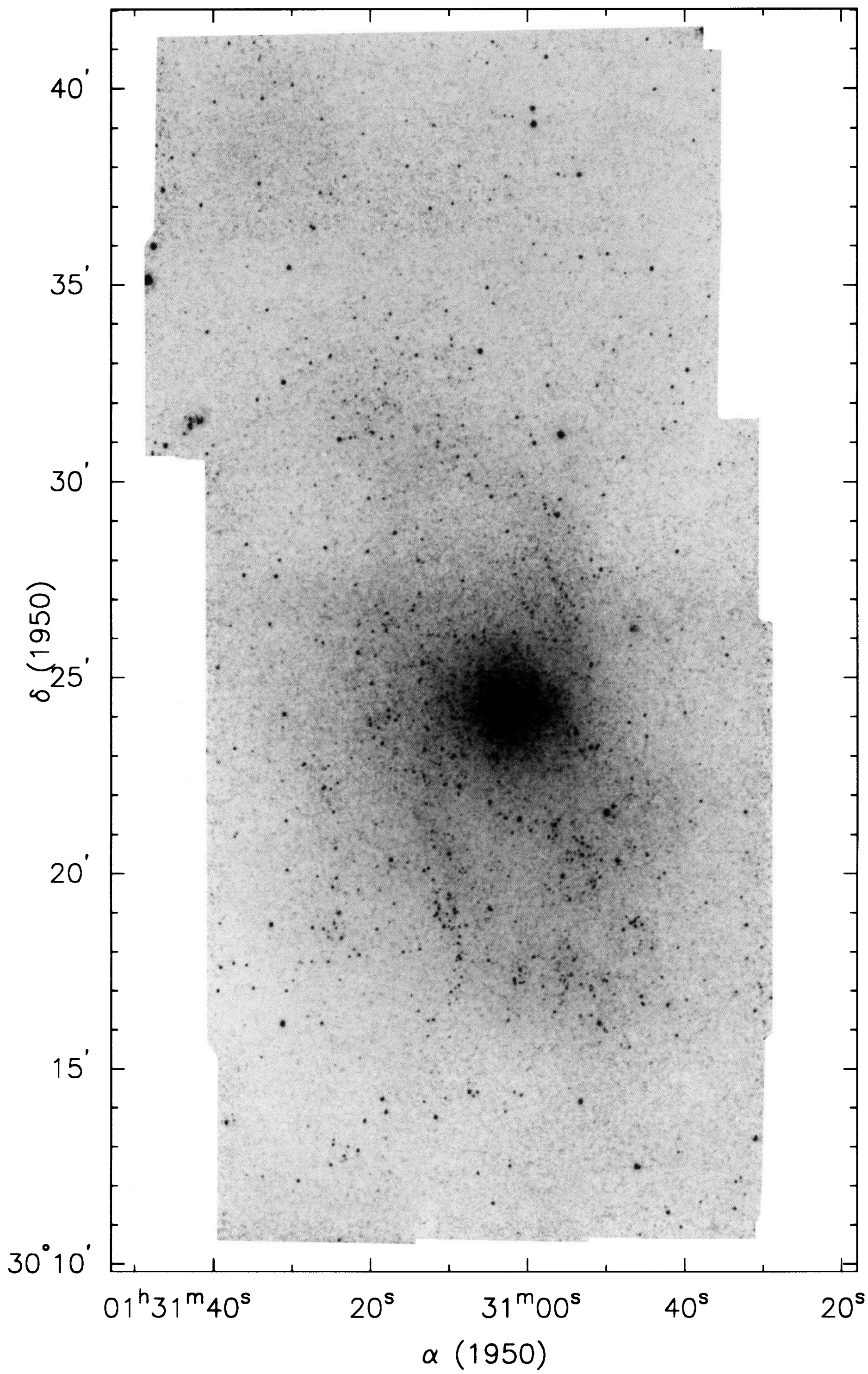

FIG. 1c

REGAN & VOGEL (see 434, 537)

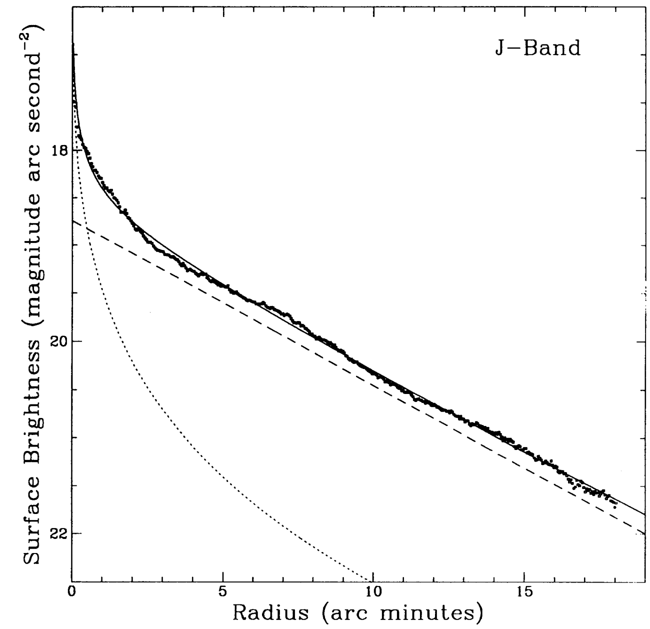

FIG. 2*a*

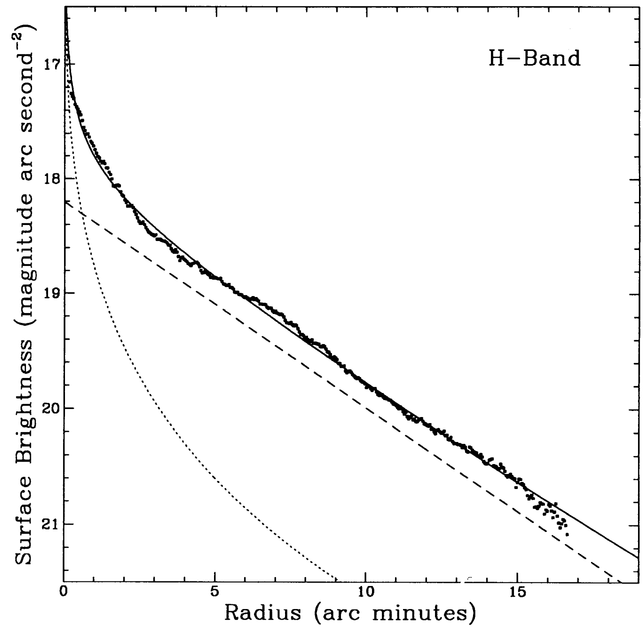

FIG. 2*b*

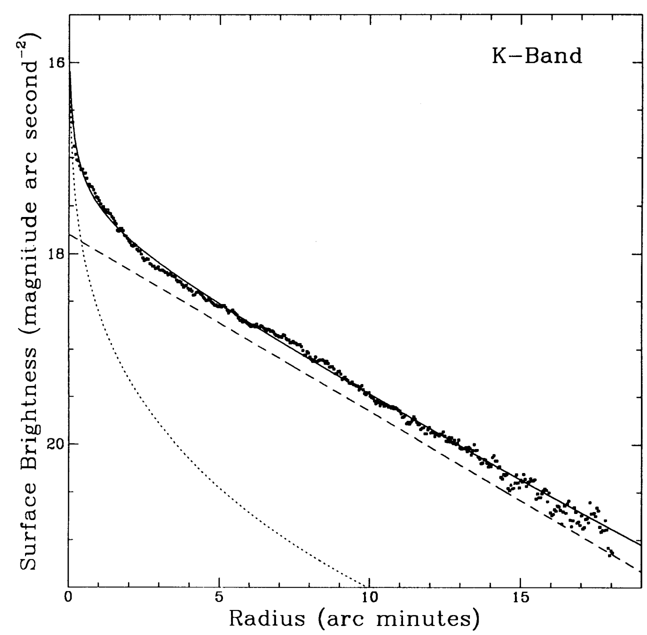

FIG. 2*c*

FIG. 2.—Plot of near-infrared surface brightness vs. radius for M33. In these plots the dashed line shows the contribution of the disk component of the model, the dotted line shows the contribution of the spheroid component, and the solid line shows the composite model. (*a*) *J*-band (λ midpoint = 1.27 μm), (*b*) *H*-band (λ midpoint = 1.67 μm), (*c*) *K*-band (λ midpoint = 2.22 μm).

15′ × 30′ (3.6 × 7.2 kpc on the sky) imaged region. The central region of the galaxy is more prominent than in visual images, suggesting the presence of a spheroidal stellar distribution (bulge or halo). The two main spiral arms, although faint, are also evident.

3.1. *Surface Photometry*

Before determining the surface brightness distribution, the galaxy was deprojected assuming an inclination of 56° and a position angle of 23° (Deul & van der Hulst 1987). The median brightness, I, was calculated as a function of radius, r, measured to the center of annuli of width 3″, and is shown in Figures 2*a*–2*c*. Smaller annuli do not change the results. The light distribution of the stellar disk is fitted by

$$I(r) = I_0 \exp\left(-\frac{r}{k_\lambda}\right) + C\,, \qquad (5)$$

where I_0 is the central intensity, k_λ is the scale length at a given wavelength, and C is an offset included to confirm the estimate of the observational zero point discussed in § 2; as expected, C is small. We limited the fit to $r > 4'.5$ to minimize the effect of the well known central luminosity excess. The mosaics were then set to the correct zero point derived from equation (5). As a check of the zero point offset we compared our *H*-band aperture photometry to the results of Aaronson, Mould, & Huchra (1980); the zero point required for consistency with the Aaronson et al. (1980) photometry agrees with the zero point derived from equation (5) to within 2 counts pixel^{-1}.

After subtracting the exponential disk, a central emission excess reasonably modeled by an $r^{1/4}$ distribution remains. The fainter isophotes of this spheroidal stellar distribution center on the semistellar nucleus to within 2″, while the center of some of the brighter isophotes are offset from the nucleus to the south. The brighter isophotes are in loose agreement with MOR who found that the isophotes in *H* band were offset from the semistellar nucleus by 20″ to the southeast. The offset in the brighter isophotes is primarily due to Association 1. Thus, the center of the fainter isophotes is more indicative of the center of the spheroidal distribution.

The existence of two light distributions covering our entire mosaics led us to solve for a simultaneous de Vaucouleurs $r^{1/4}$ distribution and exponential disk by using the deprojected surface photometry as input to a χ^2 minimization routine that solved the equation

$$I(r) = I_0 \exp\left(-\frac{r}{k_\lambda}\right) + I_e \exp\left\{-7.67\left[\left(\frac{a \cdot r}{r_e}\right)^{1/4} - 1\right]\right\}, \qquad (6)$$

TABLE 1

DISK SURFACE PHOTOMETRY RESULTS

Parameter	J Band	H Band	K Band
Scale length of the disk	6′.3	6′.1	5′.8
Central surface brightness of the disk[a]	18.75	18.21	17.80

[a] Magnitude per square arcsecond.

where r_e is the radius inside of which is half of the total light from the bulge, I_e is the spheroidal intensity at r_e, and a is a correction factor for the effect of deprojecting a spherical spheroid. The correction factor, a, only depends on the inclination angle, i, of the galaxy

$$a = \sqrt{\frac{(1 + \cos^2 i)}{2}} . \tag{7}$$

To avoid contamination by the semistellar nucleus (O'Connell 1983; Kormendy & McClure 1993) we avoid the inner 6″ when fitting equation (6). The composite model is shown as a solid line in Figure 2, while the disk is a dashed line and the bulge is a dotted line. Including uncertainties in the zero point, we estimate that the rms uncertainty in the scale lengths of the disk are 0′.3, 0′.3, and 0′.4 for J, H, and K respectively. The surface brightness and scale lengths determined for the disk are shown in Table 1. Table 2 shows that the scale lengths of 5′.8 to 6′.3 measured for the J, H, and K bands are within the range obtained for other bands for M33. However, some trends are evident. The near-infrared scale lengths (including 12 μm) are shorter than both the optical (7′.6 to 9′.0) and the far-infrared (6′.3 to 7′) scale lengths. Since the far-infrared is tracing dust emission (Rice et al. 1990) while the near-infrared and optical bands are tracing stars, the far-infrared will not be discussed further. The overall trend of decreasing scale lengths with increasing wavelength seen from optical to the near-infrared bands can be explained in part by extinction. A trend of decreasing extinction with galactocentric radius has been observed in M33 (Wilson, Freedman, & Madore 1990; Regan & Wilson 1993). If we assume that the extinction drops off exponentially, as the molecular gas does in many spiral galaxies (Scoville & Young 1983), the observed surface brightness of an exponential stellar disk can be represented as

$$\mu_\lambda(r) = \mu_{0\lambda} + 1.0857\left(\frac{r}{k}\right) + A_{0\lambda} \exp\left(\frac{-r}{k_e}\right) , \tag{8}$$

where μ_λ is the observed surface brightness in magnitudes, $\mu_{0\lambda}$ is the true central surface brightness in magnitudes, $A_{0\lambda}$ is the central extinction, k is the true scale length of the disk, and k_e is the scale length of the extinction. If the exponential decrease in extinction is expanded and only the first two terms are retained, then we get

$$\mu_\lambda(r) = \mu_{0\lambda} + 1.0857\left(\frac{r}{k}\right) + A_{0\lambda}\left(1 - \frac{r}{k_e}\right) , \tag{9}$$

If we now convert equation (5) from linear surface brightness units to magnitude units,

$$\mu_\lambda(r) = \mu_{0\lambda m} + 1.0857\left(\frac{r}{k_\lambda}\right) , \tag{10}$$

where $\mu_{0\lambda m}$ is the measured value of $\mu_{0\lambda}$, and then equate equations (9) and (10) we find that at $r = 0$,

$$\mu_{0\lambda} = \mu_{0\lambda m} + A_{0\lambda} . \tag{11}$$

Therefore, in general,

$$k_\lambda = k\left(1 - \frac{A_{0\lambda}}{1.0857}\frac{k}{k_e}\right)^{-1} . \tag{12}$$

$A_{0\lambda}$ can be replaced by $[A(\lambda)/A(V)](A_{0V})$, where $A(\lambda)/A(V)$ is the extinction relative to the visual extinction and A_{0V} is the central extinction in V band. We can obtain an estimate of A_{0V} from Wilson (1990), where the average $B-V$ color excess for the central OB associations in M33 is shown to be 0.3. This leads to an estimate of A_{0V} of 0.9 for the central region of M33. We can then make the substitution $A_{0V} = 0.9$ and solve for k_λ

$$k_\lambda = k\left[1 - 0.821\,\frac{A(\lambda)}{A(V)}\frac{k}{k_e}\right]^{-1} . \tag{13}$$

As $A(\lambda)/A(V)$ goes to zero, k_λ goes to k. We have used the relative extinctions of Cardelli, Claxton, & Mathis (1989) and the previous measurements of scale lengths in M33 as input to a least-squares routine to obtain estimates of the true scale length and the extent of the extinction. The model predicts that the true scale length of the stellar disk in M33 is 5′.3. Table 3 shows the measured values and predicted values of k_λ from this model. Although this model is simple (for example, it ignores forward scattering and the fact that the dust and stars are mixed with different scale heights), it is nonetheless apparent that the variation in scale lengths can be attributed in part to

TABLE 2

DISK SCALE LENGTHS

Wavelength	Scale Length	Source
B (0.44 μm)	8′.5 ± 0′.2	1
V (0.55 μm)	9.1	2
R (0.7 μm)	8.2	2
r (0.65 μm)	9.6	3
I (0.9 μm)	7.4	2
J (1.2 μm)	6.3 ± 0.3	4
H (1.6 μm)	6.1 ± 0.3	4
K (2.2 μm)	5.8 ± 0.4	4
12 μm	5.3 ± 0.2	5
12 μm	5.6 ± 0.2	6
25 μm	5.3 ± 0.2	5
60 μm	6.3 ± 0.2	5
100 μm	7.0 ± 0.2	5

SOURCES.—(1) de Vaucouleurs 1959; (2) Guidoni, Messi, & Natali 1981; (3) Kent 1987; (4) this paper; (5) Rice et al. 1990; (6) Bothun 1992.

TABLE 3

PREDICTED VERSUS ACTUAL SCALE LENGTHS

Wavelength	Measured Scale Length	Predicted Scale Length
V (0.55 μm)	9′.1	9′.8
R (0.7 μm)	8.2	8.3
r (0.65 μm)	9.6	8.3
I (0.9 μm)	7.4	7.1
J (1.2 μm)	6.3	6.5
H (1.6 μm)	6.1	6.2
K (2.2 μm)	5.8	6.0
12 μm	5.3	5.7

extinction and that K-band measurements will provide the scale length least affected by dust extinction. The effect of including forward scattering in the optical can be quite large (Witt, Thronson, & Capuano 1992). At low optical depths including forward scattering will lessen the effective optical depth and would lessen the expected trend of decreasing scale length with increasing wavelength. Radial variations in age or abundance can also lead to color variations, so dust extinction may not be the sole cause of the variation, but must contribute at some level. Since the near-infrared is also less affected by age (§ 4) and abundance variations (Aaronson et al. 1978), the near-infrared yields the most accurate determination of the scale length of the stellar mass distribution.

3.2. *Spiral Arms*

To enhance the contrast of nonaxisymmetric features, we created a model disk and a model spheroid using the parameters for the disk and $r^{1/4}$ distribution obtained in § 3.1. We then subtracted the model disk and spheroid from the galaxy mosaics to form residual images (Figs. 3*a*–3*c* [Pls. 27–29]), revealing nonaxisymmetric features and other aspects of the observed light distribution not well represented by our spheroid and exponential disk model. Although the two main spiral arms of M33 are plainly visible in the galaxy mosaics (Fig. 1), the residual mosaics (Fig. 3) show the arms even more clearly.

To determine the strength of the enhancement in infrared emission in the spiral arms, we measured the intensity contrast between the arm and interarm regions. We chose 10 regions of 11 × 11 pixels (15″3 × 15″3) in both the northern and southern spiral arms and matched each region with a pair of interarm regions on opposite sides of the arm at equal galactocentric radii. In each of these regions we determined the median and the mean intensity. The median should be more representative of the true underlying intensity since it is less sensitive to contamination due to isolated young bright K supergiants. Table 4 shows the arm/interarm contrasts for the northern and southern spiral arms calculated using both the mean and the median. Inspection of the table reveals that the mean intensity ratio is 0.02 to 0.06 higher than the median intensity ratio, which is equivalent to a 10%–30% overestimate of the contrast. At the location of known OB associations the estimate of the contrast obtained with the mean can be more than 50% higher than the estimate obtained by using the median.

We converted the mean intensities in the northern and southern spiral arms to magnitudes from which we determined colors in the arm and interarm (Table 5). The $J-H$ colors show no variation between any of the regions. The variation in the $H-K$ colors is probably due to systematic problems with the K band flat field; these effects average out in the surface photometry.

TABLE 4

ARM/INTERARM DENSITY CONTRASTS

Area and Method	J Band	H Band	K Band
Northern arm: mean	1.35 ± 0.04	1.30 ± 0.04	1.39 ± 0.10
Northern arm: median	1.27 ± 0.04	1.25 ± 0.03	1.30 ± 0.08
Southern arm: mean	1.29 ± 0.08	1.30 ± 0.10	1.28 ± 0.09
Southern arm: median	1.26 ± 0.06	1.28 ± 0.07	1.27 ± 0.07

TABLE 5

INFRARED COLORS OF ARM AND INTERARM REGIONS

Color	N Arm	N Interarm	S Arm	S Interarm
$J-H$	0.54	0.57	0.55	0.55
$H-K$	0.22	0.14	0.36	0.36

3.3. *Inner Stellar Disk*

The residual mosaics (Fig. 3) also reveal that the structure of the spiral arms changes significantly as the arms approach a radius of 1′5 east and west of the nucleus. Figure 3 shows a bar-shaped region inside a radius of 1′5 connecting the east and west spiral arms through the nucleus. We will discuss possible interpretations of this luminosity excess as either a bar or a steepening in the pitch angle of the spiral arms in § 5.2.

4. NEAR-INFRARED EMISSION: TRACER OF THE OLD STELLAR DISK OR OF MASSIVE STAR FORMATION?

Because the near-infrared is less affected by extinction and by light from young OB stars than the visible, it is generally assumed that the near-infrared is a good tracer of the distribution of light from the old stellar population. A potential problem is that as young OB stars evolve, they move off the main sequence and become red supergiants. These red supergiants are very luminous and could contribute a significant amount of the total light seen in the near-infrared, leading to an enhancement where there has been recent star formation. A recent study of M51 using the gravity-sensitive CO bands indicated that in general the young infrared bright stars do not significantly add to the infrared emission (Rix & Rieke 1993). However, M51 has unusually strong stellar arms and may not be representative of most galaxies.

A simple inspection of M33 optical and infrared images shows that OB associations identified in the optical images are also prominent in the infrared images, although the stars seen in the infrared are ∼15 million yr old supergiants, *not* the OB stars seen in the optical. M33 provides a unique opportunity to investigate the contribution of recent star formation to the infrared emission. The location, sizes, and boundaries of many OB associations have been determined in M33 (Wilson 1990; Regan & Wilson 1993) allowing us to determine the location and amount of recent star formation. Also, the relatively nearby location allows some individual stars to be resolved and their colors determined. Our photometry of several isolated infrared stars within OB associations reveals them to be the expected red supergiants. The median-mean comparison performed in § 3.2 shows that resolved red stars contribute to the overall emission. This comparison generates a lower bound to the true contribution of individual stars since if there are enough supergiants in a region they will bias even the median.

Toward OB associations, we observe a typical infrared enhancement in K-band emission of 40% above the background disk. This enhancement is twice as large as in arm regions where OB associations are not present. Therefore, toward typical OB associations recent star formation leads to a 20% enhancement above the disk emission. For example, in the section of the southern spiral arm discussed in Regan & Wilson (1993) the covering factor of OB associations is 25%. Thus, from star formation alone we would expect to see an arm/interarm emission contrast ratio of 1.05.

Therefore, our observations reveal that the near-infrared emission is enhanced in regions of recent star formation. We also resolve some of the individual stars that cause the near-infrared emission and, based on their colors, conclude that

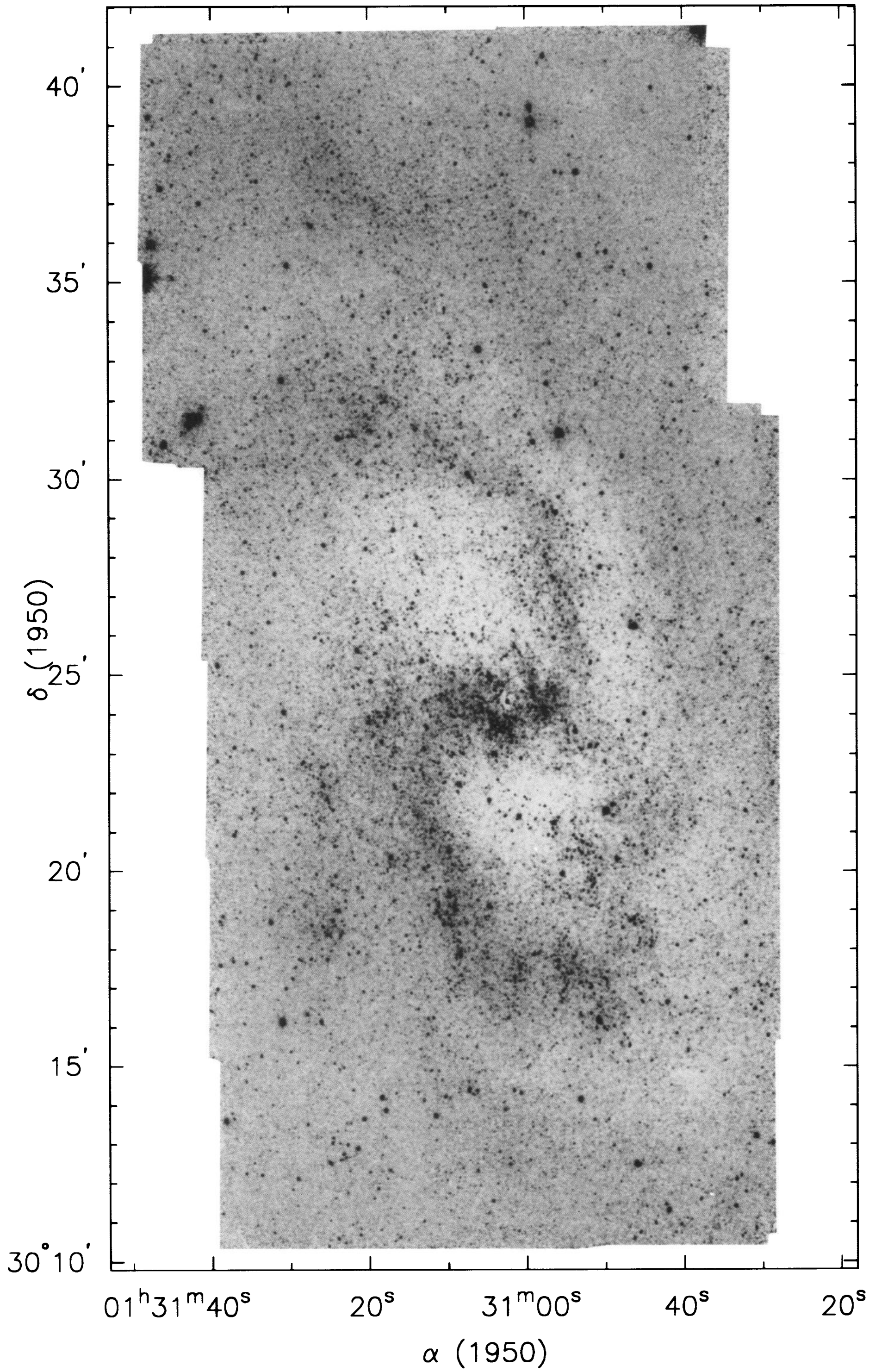

FIG. 3a

FIG. 3.—Residual mosaics of the inner 15′ × 30′ of M33 after an exponential disk and spheroid have been subtracted. The spiral arms and the bar are apparent in these images. (*a*) *J*-band (λ midpoint = 1.27 μm), (*b*) *H*-band (λ midpoint = 1.67 μm), (*c*) *K*-band (λ midpoint = 2.22 μm).

REGAN & VOGEL (see 434, 540)

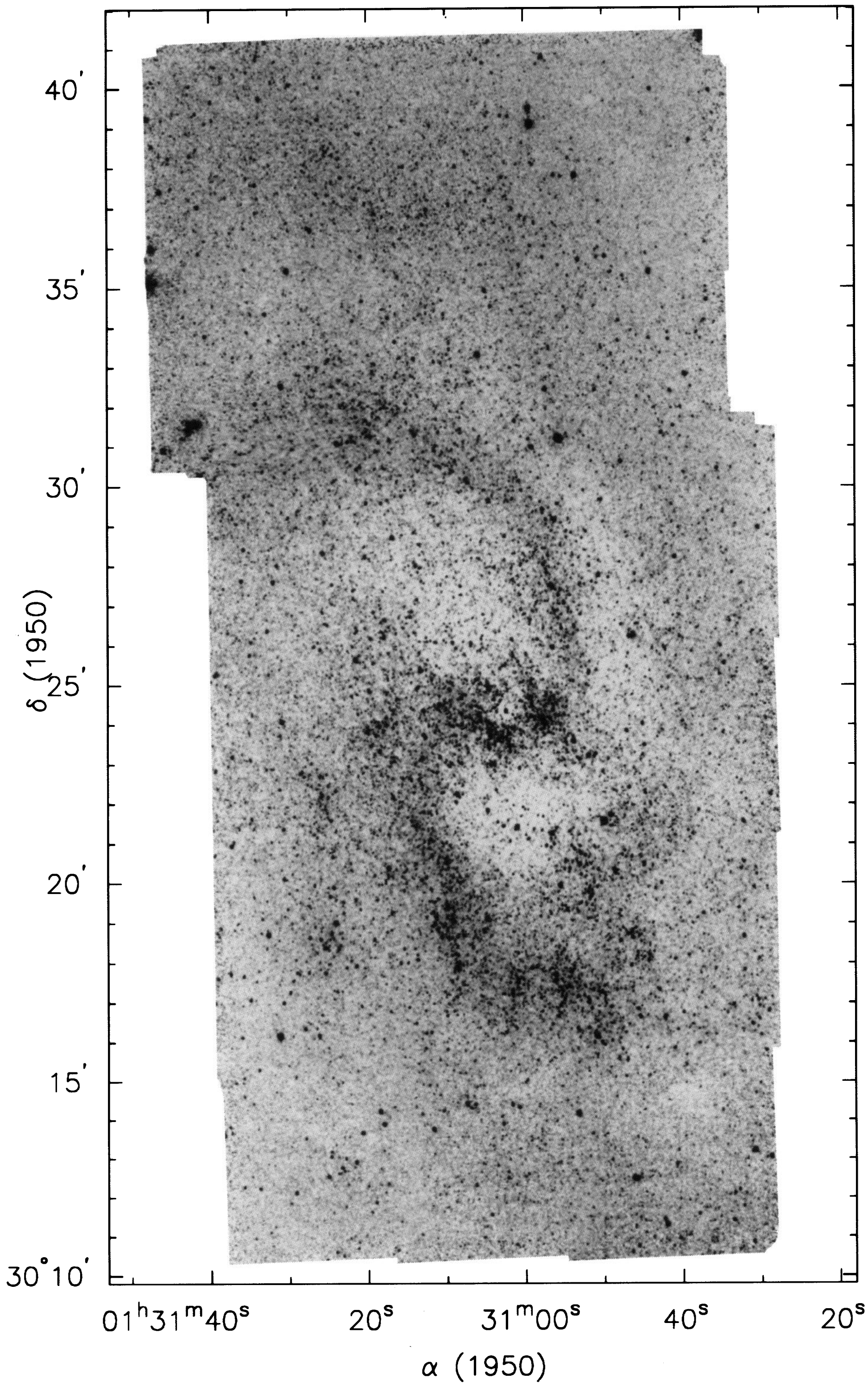

FIG. 3b

REGAN & VOGEL (see 434, 540)

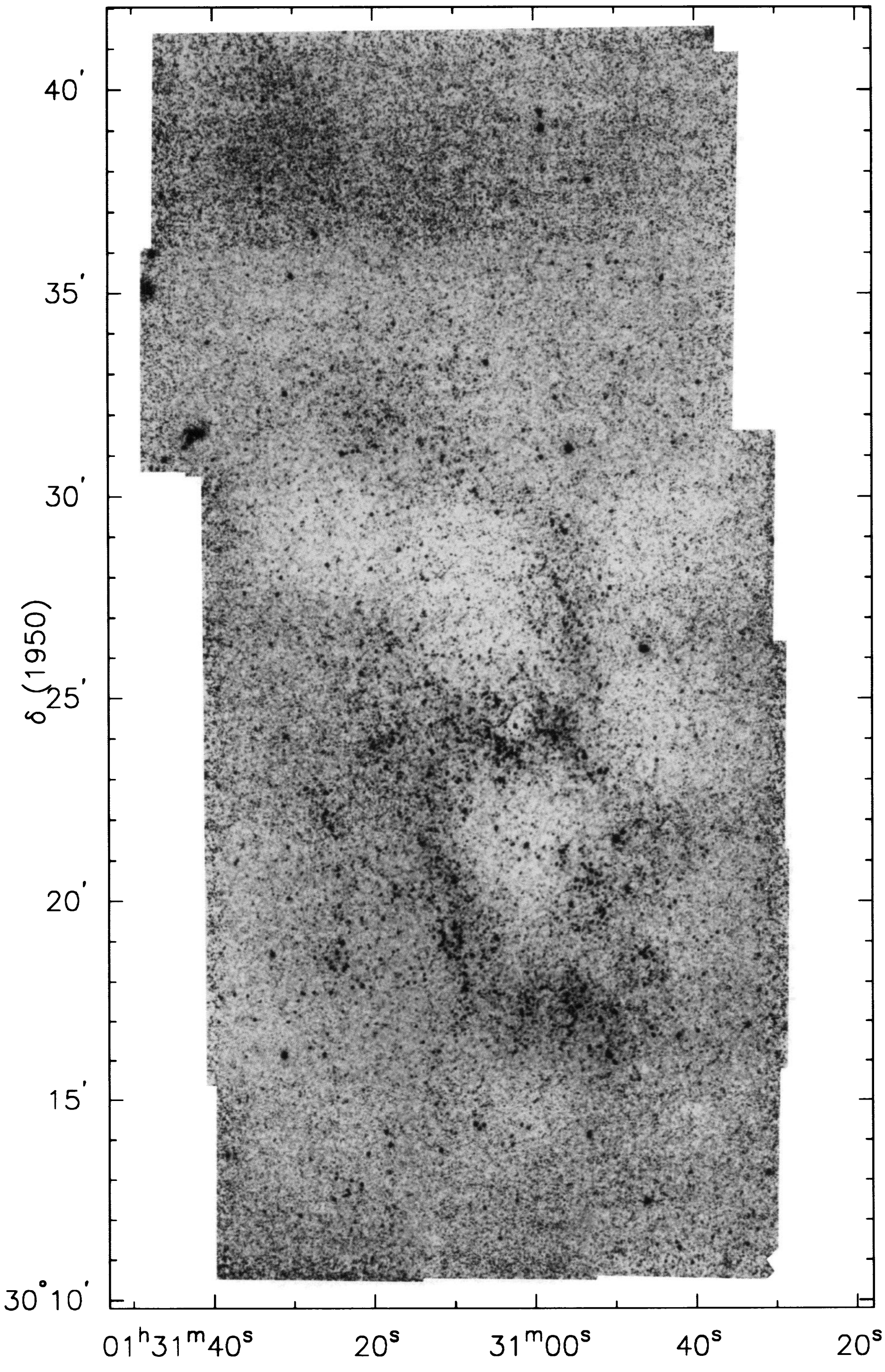

FIG. 3c

REGAN & VOGEL (see 434, 540)

they are the expected red supergiants that result from the evolution of young massive stars.

To help explain the observed enhancement, we can compare the enhancement in K-band emission due to recent star formation to that predicted by recent population synthesis models (Bruzual & Charlot 1993). For example, the largest association in the southern spiral arm of M33 has a mass of 5120 $M_\odot$ in stars more massive than 20 $M_\odot$ (Regan & Wilson 1993). Using a Miller and Scalo IMF (Miller & Scalo 1979) we arrived at a total mass of recently formed stars of 6.3×10^4 $M_\odot$. Note that the shape of the IMF is not important, since only the high-mass stars contribute to the K-band enhancement, and the star formation rate is estimated by using only OB stars. Since this amount of star formation is estimated from the blue stars which have a lifetime of less than 10^7 yr, we get a star formation rate of 6.3×10^{-3} $M_\odot$ yr^{-1}. We then modify the models of Bruzual and Charlot to reflect this rate of star formation over a period of 2×10^7 yr to take into consideration the continuous star formation seen in OB associations (Blaauw 1964; Elmegreen & Lada 1977; Doom, De Greve, & de Loore 1985; Massey et al. 1989; Regan & Wilson 1993). The results of the models are not sensitive to the actual duration of the star formation since longer periods of star formation only smooth out the period of peak emission. We then spread the light out over the surface area of the association and add the distance modulus of M33, yielding Figure 4, which shows the predicted K-band surface brightness of the association versus time. Using the average K surface brightness of the underlying disk at the galactocentric radius of the association, we determine the predicted percent enhancement to the underlying disk caused by the recent star formation (Fig. 5). The enhancement is negligible until 10^7 yr, which is when the red supergiants start to appear. Note that although we use the largest association in this exercise, the result is similar when other associations are used because their mass surface densities are similar. In summary, the predicted enhancements in the surface brightness are similar to what we observe, which implies that the red supergiants are affecting the infrared emission where there has been recent star formation.

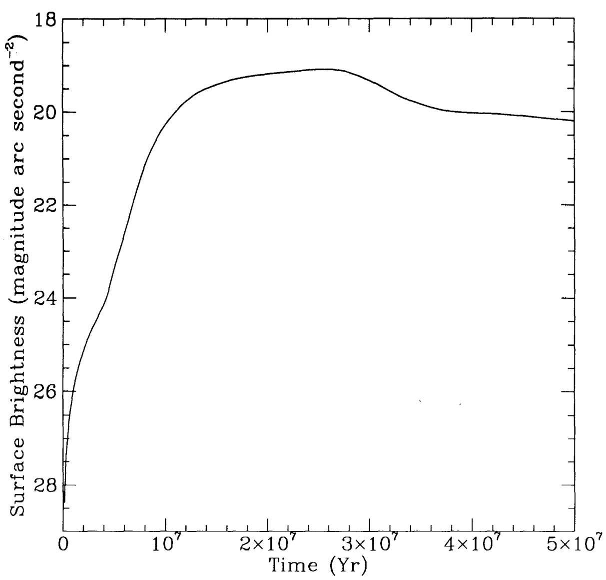

FIG. 4.—Plot of K surface magnitude vs. time for a sample association assuming that the star formation is spread out over 2×10^7 yr.

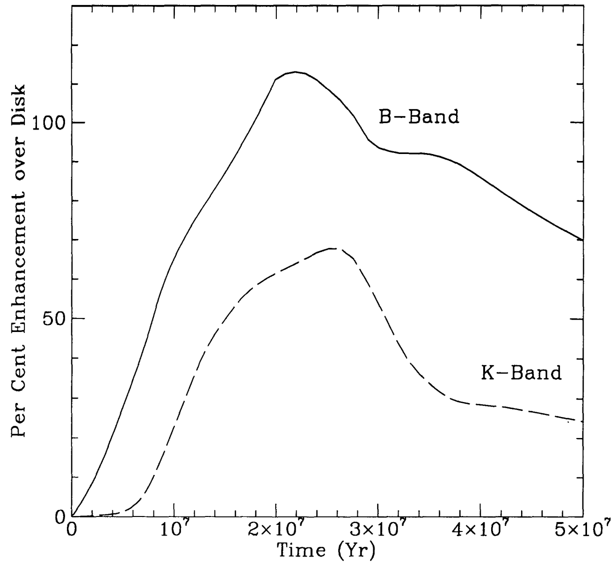

FIG. 5.—Plot of the enhancement over the background disk of a sample OB association assuming that the star formation is spread out over 2×10^7 yr, and that the association is at a distance of one disk scale length. The solid line is the B-band enhancement; the dashed line is the K-band enhancement assuming a $B-K$ color of 2.9 for the disk.

The models can also be used to determine the enhancement that would be seen in B band (Fig. 5). Here the enhancement starts earlier and reaches a higher peak although the peak in B band is only 1.5 times the peak in K band. Evidently, peak enhancements caused by star formation are almost as large in K band as in B band (i.e., $\frac{2}{3}$ of the B-band enhancement). Thus, K-band emission is not significantly better than B band in avoiding contamination from recent star formation.

The question therefore arises as to how to estimate the amount of contamination from recent star formation. One way is to use the CO band head to estimate the amount of light from supergiants (Rix & Rike 1993). A second method would be to use the localized nature of OB associations to remove the local peaks in the light distribution. A third would be to use the models of Bruzual & Charlot, combined with measurements of the Hα luminosity for a region to estimate the K-band luminosity due to recent and ongoing star formation. Because the Hα and K-band emission do not peak at the same time, this method will apply only to large areas where we can average over a significant number of star-forming regions. If $L_{\mathrm{H}\alpha}$ is the Hα luminosity in ergs s^{-1} and M_K is the peak K-band absolute magnitude due to red supergiants,

$$M_K = -1.7 - 2.5 \log\left(\frac{L_{\mathrm{H}\alpha}}{8.4 \times 10^{33}}\right). \quad (14)$$

The association will obtain this peak luminosity only for a short period of time, but the absolute magnitude will be brighter than

$$M_K = -2.5 \log\left(\frac{L_{\mathrm{H}\alpha}}{8.4 \times 10^{33}}\right) \quad (15)$$

from 10^7 to 10^8 yr. Note that this is the average enhancement. Age and gas content differences will cause individual associations to vary from this estimate.

We can use this method to estimate the amount of K-band enhancement in the region of Association 1 of Wilson (1990) due to recent star formation. We measure the Hα flux in the region of Association 1 of Wilson (1990) using the Hα images of the central region of M33 of Wilson & Scoville (1991), and obtain an Hα luminosity of 4.59×10^{37} ergs s^{-1}. By using equation (13) we obtain a peak K-band luminosity due to recent star formation of $M_K = -11$. Photometry of the residual K-band mosaic in the region of Association 1 yields an absolute magnitude of −13.8. Thus, unless the Hα flux of Association 1 is unusually low, less than 10% of the excess K-band light can be attributed to recent star formation and the central disk light excess is not caused by recent star formation.

In summary, K-band enhancements due to star formation are roughly one-half that of the optical enhancement and therefore should not be neglected. The contamination by recent star formation can be estimated by using the CO band head or Hα emission, or avoided by excluding localized regions of K-band enhancement. Thus, the major advantage of K-band emission for tracing the stellar mass distribution is the low extinction compared to optical.

5. DISCUSSION

5.1. *The Spheroid*

The *JHK* images of M33 presented here show a luminosity excess above the disk emission in the central 1′–2′, as seen in previous observations. The luminosity excess has been attributed to spiral arms (Kent 1987), an extended semistellar nucleus (O'Connel 1983), a diffuse halo (Bothun 1992), and a bulge (Boulesteix et al. 1979; Bothun 1992; MOR). The late Hubble type of M33 and the presence of the bright star-forming blue nucleus (O'Connell 1983; Kormendy & McClure 1993) have made it difficult to distinguish between these possibilities. The observation of a luminosity excess in the infrared by MOR and by us does not by itself rule out excess star formation, as in spiral arms, since this would produce an infrared excess (see § 4), and the lower extinction in the infrared might make the region more prominent in the infrared than in the optical. However, the *smoothness* of the central emission (Fig. 1) in comparison to other bright regions such as the spiral arms and OB association does suggest an older more numerous population of stars such as is found in a spheroidal distribution.

Boulesteix et al. (1979), using B-band photometry, fit a $r^{1/4}$ distribution with $R_e = 2\overset{'}{.}75$, diffuse for a centrally concentrated bulge, and with $I_e = 24.5$ mag, 2 mag fainter than most bulges (Kent 1985). In a more detailed study, Bothun (1992) derived similar parameters for the central luminosity excess and noted that it was difficult to distinguish between a bulge and a halo. He suggested that the low surface brightness (including at 12 μm) implied a halo. MOR detected a luminosity excess in the H band in the central 1′ and prefer to attribute the excess to a bulge. Although the precise values of R_e and J_e determined by MOR are not given, they state that the parameters are similar to those determined by Bothun (1992).

TABLE 6

SPHEROIDAL PHOTOMETRY RESULTS

Parameter	*J* Band	*H* Band	*K* Band
R_e	$8'^{+3}_{-2}$	$8'^{+3}_{-2}$	$8'^{+3}_{-2}$
I_e[a]	23.42	22.84	22.63

[a] Magnitude per square arc second.

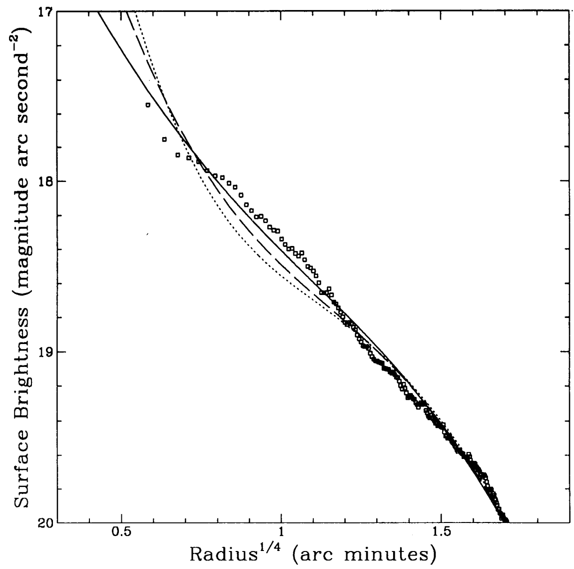

FIG. 6.—Plot of surface brightness vs. radius$^{1/4}$ for J band. The solid line represents our best fit model ($R_e = 17'$), while the dashed line represents the model where R_e was constrained to be 3′, and the dotted line represents the model where R_e was constrained to be 1′. In all of the models the inner 6″ was excluded to prevent contamination by the semistellar nucleus.

For simplicity, we will consider whether the entire spheroidal light distribution can be fitted by a single spheroidal distribution. The spheroid brightness at $R = 24'$ can be obtained from the luminosity function of Mould & Kristian (1986) using the expected near-infrared colors of their halo stars. Including this as a data point in our fit we obtain the parameters for the spheroid shown in Table 6. The reduced χ^2 for the J, H, and K fits is 5.3, 6.0, and 6.5, respectively. Figure 6 shows that although some departures from a simple $r^{1/4}$ law and exponential disk are evident (see the residuals plotted in Fig. 7), the fit is better than any previously published fit, including in the inner 1′. Figure 7 shows the residual light after the fit to equation (6) versus radius$^{1/4}$ for the J-band surface

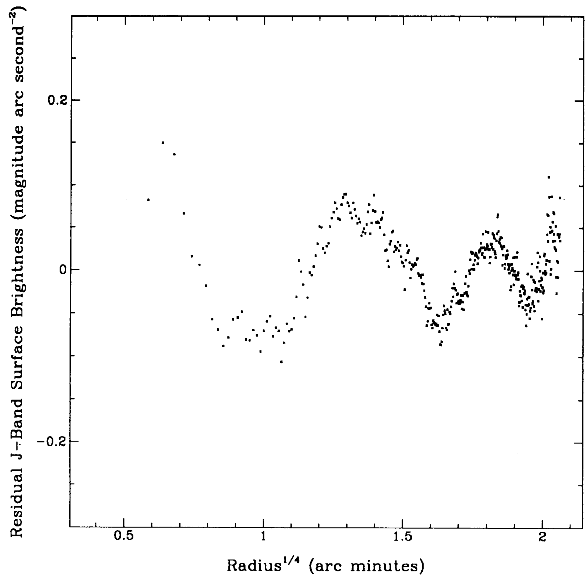

FIG. 7.—Plot of residual surface brightness after we subtract an exponential disk and a spheroid vs. radius$^{1/4}$ for J band.

photometry. These oscillating residuals have been seen before in ellipticals (Jaffe 1983) and indicate that the $r^{1/4}$ and exponental disk model is too simple. The oscillations are relatively smooth and extend throughout the regions dominated by the spheroid and by the disk. The oscillations in the disk may be due to spiral arms, but this cannot explain why they occur in the central arc minute where the arms are no longer present. Since the model is a bit high in the inner 10″, the fit would not be significantly improved by including a compact bulge. Therefore, if a compact bulge, such as advocated by MOR, is present it does not make a large contribution to the spheroidal light.

The value of $R_e = 8'$ (2 kpc) is close to the observed value of R_e for the spheroid of the Milky Way of 3 kpc (de Vaucouleurs & Pence 1978). Since the colors predicted by Bruzual & Charlot (1993) for a population which has undergone no star formation for 10^{10} yr ($B-J = 3.0$, $B-H = 3.6$, and $B-K = 3.9$) are very similar to those observed in ellipticals and S0 galaxies (Gavazzi & Trinchieri 1989), we use them to derive a very similar B-band surface brightness of $I_e = 26.5$ for each of the three near-infrared bands. This yields a value for the spheroid/disk (S/D) ratio of 0.03, somewhat higher than the bulge/disk ratio of 0.01 to 0.02 previously calculated for M33 (Bothun 1992). Note that if we used bluer colors as would be implied by the recent star formation reported by MOR we would get a more luminous spheroid and an even higher spheroid to disk ratio.

The larger values of R_e and S/D obtained from our infrared data cannot be attributed to a decrease in extinction with radius since this would produce a steeper light distribution in the infrared compared to the optical. The estimate for A_{0V} of 0.9 obtained in § 3.1 yields a value of $A_{0K} = 0.1$. This level of extinction in K is too low to explain the shallow slope of the light distribution in the inner regions of the galaxy. Since small changes in the slope of log (I) versus $r^{1/4}$ (Fig. 6) imply large changes in the fit value of R_e (see eq. [6]), the uncertainty in R_e is large. Figure 6 shows the best fit to the J-band surface photometry along with two other fits where R_e was constrained to be 1′ and 3′. The $R_e = 8'$ solution fits the data much better in the 4″–10″ region where we have the most leverage on it, while the smaller values of R_e predict a much steeper gradient in the surface brightness than is seen.

We can derive an estimate of the total V-band luminosity for our spheroid using equation (5) of Burstein (1979) by converting our J, H, and K values of I_e to V band using the expected spheroid colors from above, yielding $-16.5 < M_V < -15.0$, when we include the uncertainties in the measurements. Note that this spheroid is quite diffuse and we are assuming that it follows the same $r^{1/4}$ law out to several R_e to derive the total luminosity. Although our estimate of the spheroid luminosity is uncertain, the observations of Mould & Kristian (1986) at $R = 24'$ do give us a data point at several R_e. This estimate of the luminosity is more luminous than the range of values derived by Bothun (1992) of $-15 < M_V < -13.8$. Bothun's (1992) 12 μm upper limit to the spheroid luminosity was derived using $R_e = 1'$. Our data show that this value is too small, and since a larger value of R_e with the same I_e implies a more luminous spheroid, we need to rederive the upper limit. When we use our value of R_e and solve for I_e with the 12 μm photometry we obtain an upper limit of $M_V = -16$ using the colors of a K5 star. M_V is important because a relationship between S_V, the ratio of the number of globular clusters in a galaxy to the total V-band luminosity of its spheroidal distribution (M_V), and the Hubble type of the galaxy has been observed (Harris & van den Bergh 1981; Harris 1988). S_V has been measured in ellipticals and in early spirals and has been shown to be in the range of 3–5 in early spirals (Harris 1988), but except for M33 it has not been measured in late spirals. Using the range in total luminosity of M33 provided by Bothun (1992) and the number of globular clusters observed in M33 of 20–25 (Christian & Schommer 1988; Schommer et al. 1991) results in $20 < S_V < 72$. In contrast, our values of M_V yield a range of $5 < S_V < 25$. This is closer to what is seen in early type spiral galaxies. Some of the excess in S_V seen in M33 is because it is closer. Thus, M33 may not have an unusual number of globular clusters relative to its spheroid luminosity.

In summary, we detect a $r^{1/4}$ light distribution in the central region of M33 with a value of $R_e = 8'$, which although not precisely determined is clearly significantly larger than previously reported estimates. This spheroid has a larger value of M_V than previously obtained, leading to a value of S_V closer to the range seen for spiral galaxies. Measurements of the central region of M33 with better seeing and smaller pixels may separate the effect of the nucleus and allow surface brightness measurements to extend into smaller radii, thus better constraining the values of R_e and I_e. Also, detailed kinematic observations of the central region of M33 are needed to better characterize the spheroidal distribution.

5.2. *The Bar-shaped Emission in the Inner Disk: Bar or Spiral Arms?*

Although the residual images imply that there may be a bar in M33, the light distribution is not as smooth as expected from the numerous giant and main sequence stars that constitute a stellar bar. This could be the effect of the subtraction of a smooth disk when in fact the disk does not have a smooth light distribution. Thus, the variations in the disk will remain, leaving a large amount of noise relative to the weak bar. If the central region is a bar, it has a length of 3′ (700 pc), a position angle of 90°, and terminates at about the same position as was seen in the enhanced B-band images of M33 (Elmegreen et al. 1992). The emission in this region has an axial ratio of 2.8 to 1 and in the near-infrared contains 4% of the light out to a radius of 1′.5. Since the bar shaped emission only contains 4% of the light it is quite weak when compared to strongly barred galaxies which may contain as much as 40% of the light (Blackman 1983). The large association just to the south of the nucleus (Association 1 in Wilson 1990) and several other associations at the ends of the bar definitely contribute to the light but cannot account for all of the bar excess (See § 4). OB Association 1 is at an unusual location in a bar since it is not at the ends of the center where most star formation occurs in bars (Tubbs 1982). It should also be noted that most bars have a flat photometric profile, but we are not able to derive the profile for this excess due to the poor signal to noise. The most conclusive way to confirm that there is a bar is to look for the signature of the bar in the high-resolution kinematic observations.

Bothun (1992) found that short exposures of the center of M33 showed a north-south elongation, while longer exposures implied an east-west elongation. The bright north-south excess is caused by the location of association 1 just to the south of the nucleus. The east-west elongation revealed in Bothun's longer exposures is the bar-shaped excess that we see in the near-infrared.

An alternate explanation of the bar-like emission is that the spiral arms change their pitch angle at a radius of 1′.5 and continue to a radius of less than 1′. Thus, the two enhancements to the east and west of the nucleus may be just the continuation of the two spiral arms. Supporting this explanation is that if Association 1 did not exist there is little emission to the north and south of the nucleus to link together the two regions of emission excess to the east and west of the nucleus. Therefore, there is not enough evidence with surface photometry alone to conclude whether there is a bar in M33.

5.3. *Spiral Arms*

Although star formation can contribute to near-infrared emission, it cannot account for *all* of the emission enhancement observed in the major spiral arms of M33 (NI and SI of Sandage & Humphreys 1980). As shown in § 4, even toward OB associations star formation can only account for approximately half of the emission excess above the background disk observed in the spiral arms. In addition, the arms exhibit a broad relatively smooth excess even in locations where there is no evidence for star formation. Accordingly, we conclude that the two main spiral arms of M33 are not entirely gaseous but have an underlying stellar component. Interpreting this emission as a stellar mass enhancement, the contrast ratio obtained in § 3.2 implies that the ratio of the arm to interarm stellar surface density is ~ 1.2.

A kink in both the NI and SI arms is observed at a distance of $\sim 7'$ from the nucleus. Both arms generally thicken with increasing radius and exhibit a significant decrease in intensity at a radius of $\sim 9'$ (2.1 kpc). The HI rotation curve for M33 flattens near the radius at which the two arms end, ~ 9 to $10'$ (Deul & van der Hulst 1987). In the context of the Kormendy & Norman (1979) results, the coincidence of the extent of the stellar arms with the region of approximately solid body rotation suggests that the grand design arms of M33 are material arms which persist in a region of low shear. The thickening with radius of the spiral arms might be attributed to the increasing deviation from solid body rotation noted by Wilson & Scoville (1989), which would cause a shearing of the material arms. High-resolution observations of the kinematics of the inner region would help to confirm this by obtaining a rotation curve unaffected by beam smearing, by determining the absence or presence of density wave streaming, and perhaps by associating the kink in the arms with some feature of the rotation curve.

Arms NII and SII of Sandage & Humphreys (1980) are also present in our mosaics. Star formation is associated with these arms, as with the inner arms NI and SI. Emission from the NII and SII arms is weak compared to NI and SI and thus the arm/interarm contrast ratio is particularly sensitive to the adopted zero intensity level. Therefore, we cannot determine whether the NII and SII arms have an underlying stellar density enhancement.

6. CONCLUSIONS

Visual inspection of the near-infrared images along with comparisons of the arm/interarm contrast and of the near-infrared excess associated with OB associations all show that individual red supergiants contribute to the near-infrared emission in the arms. The emission is explained by population synthesis models. We find that the near-infrared light from OB associations can significantly contribute to the total light in the spiral arms. The models also show that star formation enhances the peak near-infrared emission to within 50% of the peak *B*-band enhancement, although there is a delay in the peak of the near-infrared emission of 10^7 years. This means that the primary advantage of using the near-infrared to study galactic structure is the much lower effect of extinction and that using integrated *K*-band intensities alone as a tracer of mass for galaxies further away than M33 can lead to an overestimation of the underlying mass wherever star formation is occurring. We also show how the rate of star formation estimated from the Hα can be used to predict the amount of *K*-band excess.

Although some of the arm emission in the near-infrared is due to recent star formation, we show that there is a 20% enhancement in the emission of the two inner spiral arms relative to the interarm which can be attributed to an enhancement in the stellar surface density. These stellar arms have grand-design structure and are probably material arms since the region of grand-design spiral structure coincides with the region of low shear in the rotational velocities.

The residual mosaics of M33 reveal that the bar-shaped excess may be explained either by a bar having a position angle of 90° and a length of 3′ (700 pc) or by a change in the pitch angle of the main spiral arms. This question could be resolved by high-resolution kinematic data which should show streaming motions associated with a bar.

We also derive disk scale lengths that lie between those seen in the optical and those seen in the mid-infrared. We show that when there is a trend of decreasing extinction with galactocentric radius, measured scale lengths will decrease with increasing wavelength. Thus, near-infrared scale lengths more closely reflect the underlying mass distribution in the galaxy.

The galaxy mosaics reveal a central light distribution reasonably fitted by a single $r^{1/4}$ light distribution surrounding the nucleus. We determine a much larger value for its scale length, $R_e = 8'$, than previous authors. This more diffuse spheroid is more luminous than previous estimates for the spheroid of M33. M33 was remarkable for the large number of halo-globular clusters compared to its spheroidal luminosity, e.g., large value of S_V. Using our more luminous spheroid leads to a value of S_V closer to the normal range for spiral galaxies.

We would like to thank Mike Merrill for his help with SQIID and for the creation of the IRAF SQIID package. We would like to thank Gustavo Bruzual for a copy of the Gissel population synthesis libraries. We also thank Robert Gruendl for the routines used to perform the surface photometry. We also wish to thank Chris Wilson for a copy of her Hα image of M33. We would also like to acknowledge discussions with Ken Mighell and comments from Greg Bothun. Partial support for this research was provided by NSF grant AST 93-14847, and by the State of Maryland through its contributions to the Laboratory for Millimeter-Wave Astronomy.

REFERENCES

Aaronson, M., Cohen, J. G., Mould, J., & Malkan, M. 1978, ApJ, 223, 824
Aaronson, M., Mould, J., & Hucra, J. 1980, ApJ, 237, 655
Blaauw, A. 1964, ARA&A, 2, 213
Blackman, C. P. 1983, MNRAS, 202, 379
Bothun, G. D. 1992, AJ, 103, 104
Boulesteix, J., Colin, J., Athanassoula, E., & Monnet, G. 1979, in Photometry, Kinematics, and Dynamics of Galaxies, ed. D. S. Evans (Univ. of Texas Press, Austin), 271
Bruzual, A. G., & Charlot, S. 1993, ApJ, 405, 538
Burstein, D. 1979, ApJ, 234, 435

Cardelli, J. A., Clayton, G. C., & Mathis, J. S. 1989, ApJ, 345, 245
Christian, C. A., & Schommer, R. A. 1988, AJ, 95, 704
Deul, E. R., & van der Hulst, J. M. 1987, A&AS, 67, 509
de Vaucouleurs, G. 1959, ApJ, 130, 728
de Vaucouleurs, G., & Pence, W. D. 1978, AJ, 83, 1163
Doom, C., De Greve, J. P., & de Loore, C. 1985, ApJ, 290, 185
Elmegreen, B. G., Elmegreen, D. M., & Montenegro, L. 1992, ApJS, 79, 37
Elmegreen, B. G., & Lada, C. J. 1977, ApJ, 214, 725
Fowler, A. M., Gatley, I., & Merrill, K. M. 1990, in Proc. SPIE, Infrared Technology XVI, 1341, 52
Freedman, W. L., Wilson, C. D., & Madore, B. F. 1991, ApJ, 372, 455
Gavazzi, G., & Trinchieri, G. 1989, ApJ, 342, 718
Guidoni, U., Messi, R., & Natali, G. 1981, A&A, 96, 215
Harris, W. E. 1988, in IAU Symp. 126, Globular Cluster Systems in Galaxies, ed. J. E. Grindlay & A. G. D. Philip (Dordrecht: Kluwer), 237
Harris, W. E., & van den Bergh, S. 1981, AJ, 86, 1627
Hubble, E. 1926, ApJ, 63, 236
Jaffe, W. 1983, MNRAS, 202, 995
Kent, S. M. 1985, ApJS, 59, 115
———. 1987, AJ, 94, 306
Kormendy, J., & McClure, R. D. 1993, AJ, 105, 1793
Kormendy, J., & Norman, C. A. 1979, ApJ, 233, 539
Massey, P., Garmany, C. D., Silkey, M., & Degioia-Eastwood, K. 1989, AJ, 97, 107
Merrill, K. M. 1992, private communication
Miller, G. E., & Scalo, J. M. 1979, ApJS, 41, 513
Minniti, D., Olszewski, E. W., & Rieke, M. 1993, ApJ, 410, L79 (MOR)
Mould, J., & Kristian, J. 1986, ApJ, 305, 591
O'Connell, R. W. 1983, ApJ, 267, 80
Quillen, A. C., Graham, J. R., & Frogel, J. A. 1993, ApJ, 412, 550
Regan, M. W., & Wilson, C. D. 1993, AJ, 105, 499
Rice, W., Boulanger, F., Viallefond, F., Soifer, B. T., & Freedman, W. L. 1990, ApJ, 358, 418
Rix, H. W., & Rieke, M. J. 1993, ApJ, 418, 123
Sandage, A., & Humphreys, R. M. 1980, ApJ, 236, L1
Schommer, R. A., Christian, C. A., Caldwell, N., Bothun, G. D., & Huchra, J. 1991, AJ, 101, 873
Scoville, N., & Young, J. S. 1983, ApJ, 265, 148
Tubbs, A. D. 1982, ApJ, 255, 458
van den Bergh, S. 1991, PASP, 103, 609
Wilson, C. D., Freedman, W. L., & Madore, B. F. 1990, AJ, 99, 149
Wilson, C. D., & Scoville, N. 1989, ApJ, 347, 743
———. 1991, ApJ, 370, 184
Witt, A. D., Thronson, H. A., & Capuano, J. M. 1992, ApJ, 393, 611